SIAM J. Applied Dynamical Systems
Vol. 4, No. 1, pp. 187–216

A Hamiltonian Formulation for Recursive Multiple Thermostats in a Common Timescale*

Benedict J. Leimkuhler† and Christopher R. Sweet†

Abstract. Molecular dynamics trajectories that sample from a Gibbs distribution can be generated by introducing a modified Hamiltonian with additional degrees of freedom as described by Nosé [S. Nosé, *Mol. Phys.*, 52 (1984), p. 255]. To achieve the ergodicity required for canonical sampling, a number of techniques have been proposed based on incorporating additional thermostatting variables, such as Nosé–Hoover chains and more recent fully Hamiltonian generalizations. For Nosé dynamics, it is often stated that the system is driven to equilibrium through a resonant interaction between the self-oscillation frequency of the thermostat variable and a natural frequency of the underlying system. In this article, we clarify this perspective, using harmonic models, and exhibit practical deficiencies of the standard Nosé chain approach. As a consequence of our analysis, we propose a new powerful "recursive thermostatting" procedure which obtains canonical sampling without the stability problems encountered with Nosé–Hoover and Nosé–Poincaré chains.

Key words. Nosé, Nosé–Hoover, Nosé–Poincaré, Nosé–Poincaré chains, symplectic integrator, constant temperature molecular dynamics, thermostatting

AMS subject classification. 37M15

DOI. 10.1137/040606090

1. Introduction.

The desire to provide computer simulation of molecular dynamics which samples from the canonical ensemble has led to the extensive use of momentum scaling methods to regulate the kinetic energy, and hence temperature, of the system. This is accomplished by introducing additional degrees of freedom which interact with the original system in some manner to simulate a heat bath. Most of the methods in use have their roots in the work of Andersen in [1] where constant pressure and temperature were considered. The paper of Nosé [14] constructed a family of extended dynamical systems, for which it can be shown analytically that sampling from the canonical ensemble occurs under an ergodicity assumption. For an N-body system, with original Hamiltonian $H(q,p)$, the construction was based on one additional degree of freedom with an extended Hamiltonian,

$$H_N(q,s,p,p_s) = H\left(q,\frac{p}{s}\right) + \frac{p_s^2}{2Q} + (N_f+1)kT\ln s, \tag{1}$$

where s is the new thermostatting variable, p_s the corresponding momentum, T the temperature, Q the Nosé mass, N_f the number of degrees of freedom of the original system, and k

*Received by the editors April 1, 2004; accepted for publication (in revised form) by C. Wayne July 23, 2004; published electronically February 22, 2005. This work was supported by Engineering and Physical Sciences Research Council grant GR/R03259/01.
http://www.siam.org/journals/siads/4-1/60609.html
†Centre for Mathematical Modelling, University of Leicester, Leicester LE1 7RH, England (b.leimkuhler@mcs.le.ac.uk, crs11@mcs.le.ac.uk).

the Boltzmann constant. There exist many variations of these schemes in the literature, but fundamental deficiencies have limited their use compared to alternatives, such as stochastic methods.

Nosé's method introduces an artificial scaling of the time variable which makes computation of time-correlation functions cumbersome. While correcting this deficiency, Hoover's coordinate and time transformations [6] destroy the Hamiltonian structure. To produce Hoover's method for an underlying Hamiltonian of the form

$$H(q,p) = \sum_{i=1}^{N} \frac{p_i^2}{2m_i} + V(q), \tag{2}$$

both time and coordinate transformations are applied to (1) ($p' = p/s$, $t' = \int dt/s$, $p'_s = p_s/s$, $\zeta = (1/s)ds/dt' = s\ p'_s/Q$, $\eta = \ln s$) to give

$$\frac{dq_i}{dt'} = \frac{p'_i}{m_i}, \quad \frac{dp'_i}{dt'} = -\nabla q_i V(q) - \zeta p'_i,$$
$$\frac{d\eta}{dt'} = \zeta, \quad \frac{d\zeta}{dt'} = \frac{1}{Q}\left(\sum_{i=1}^{N} \frac{{p'_i}^2}{m_i} - NkT\right).$$

More recent work by Bond, Leimkuhler, and Laird in [2], independently discovered by Dettmann [3], introduced the Nosé–Poincaré method wherein the desired rescaling of time is accomplished through transformation of the Hamiltonian itself,

$$H_{NP}(q,s,p,p_s) = s\left(H\left(q,\frac{p}{s}\right) + \frac{p_s^2}{2Q} + N_f kT \ln s - H_0\right). \tag{3}$$

Here H_0 is chosen such that the Nosé–Poincaré Hamiltonian, H_{NP}, is zero when evaluated at initial conditions. A symplectic numerical method is included in [2], and further research on integrators and applications [11, 15, 5] has helped to establish the Nosé–Poincaré framework.

A feature associated with these methods is the introduction of a parameter, Q, the Nosé mass. The selection of this mass is critical if the correct sampling is to be obtained, and it is generally calculated so that the auxiliary variable has a self-resonant frequency, estimated by linearizing the system, coincident with some natural frequency within the original system. A study of the application of the Nosé–Hoover thermostat to a large and nonintegrable system, a fluid with a Lennard–Jones potential, in [4] indicates that Nosé's criterion is satisfied. This represents a model with good coupling between different parts of the system, but for models such as Butane molecules, where the coupling between modes is poor, the correct choice of Q is not well understood.

A considerable amount of work has been done on the development of thermostats which possess desirable characteristics. These include the work of Kusnezov, Bulgac, and Bauer [9] and Martyna, Klein, and Tuckerman [13], which are generalizations of the Nosé–Hoover method intended to obtain canonical distributions for stiff systems. A number of thermostatting methods from the literature are compared in the paper by Hoover, Aoki, Hoover, and De Groot [7].

Thermostatting chains, such as Nosé–Hoover chains in [13] and Nosé–Poincaré chains [12], were introduced to generate the correct sampling for small and stiff systems, for which Nosé–Hoover and Nosé–Poincaré dynamics are not ergodic, by using additional degrees of freedom. It is noted that, for these methods, the choice of the Nosé mass for the first thermostat is less critical than in Nosé, Nosé–Hoover, and Nosé–Poincaré methods. However, the stability of the numerical implementation of Nosé–Poincaré chains is not as good as the underlying Nosé–Poincaré method as each additional thermostat controls only one other thermostat, and this is analogous to thermostatting a low dimensional system such as the harmonic oscillator. We have seen that, for the harmonic oscillator, Nosé's method has poor stability when compared to time reparametrization methods due to the artificial scaling of time introducing large time steps when the dynamics of the underlying oscillator is subject to the greatest rate of change. Each additional thermostat subsystem will have this problem as the time reparametrization is only based on the first thermostat. In addition, the low dimension of the subsystem to be thermostatted means that the expected average values for quantities based on the thermostatting variable's momentum may not be easily achievable; to overcome this, several additional thermostats are required. These problems persist regardless of the dimension of the underlying system.

In this article we develop a more general class of recursive momentum-scaling multiple thermostat methods. Extensive computer experimentation with these formulations has shown that a seemingly natural approach to parameter selection based on a simple linearization of the underlying dynamics leads to an incorrect choice of parameters. In fact, we find that the parameters (thermostat masses) in our formulation are essentially independent of the underlying system. This observation has very important advantages for the development of practical numerical approaches. The new method presented here can be applied more easily to thermostat a variety of models without the need for tedious tuning of parameters. The parameters can instead be chosen to obtain some useful property in the numerical method, such as better numerical stability or, as in [8], a desired scale separation.

To gain a better understanding of the basic methods, we examine the role of the Nosé mass in providing ergodic behavior in section 2. In section 3, a general momentum-scaling Hamiltonian formulation is introduced, and we describe as special cases the Nosé–Poincaré chains method [12] and the recursive multiple thermostat (RMT) method. The RMT method is a real-time Hamiltonian method having Nosé masses which are independent of the natural frequencies of the underlying dynamical system. A summary of the results of this paper is then discussed in section 5. An important feature of our formalism is that we remain always within the class of Hamiltonian dynamical models, for which symplectic integrators, having superior long-term stability properties, are possible. Construction of efficient schemes suitable for molecular dynamics applications is an important task. In the appendix we show that this is possible in our case, by designing an efficient Hamiltonian splitting method for RMTs.

An electronic aid to understanding the thermostatting methods described in this article is available at http://www.recursivethermostat.info.

2. Analysis of the Nosé–Poincaré method. In this section we analyze the behavior of the real-time Nosé–Poincaré method when applied to a single harmonic oscillator. By examining the auxiliary variable phase-space and modeling the system in the frequency domain, we

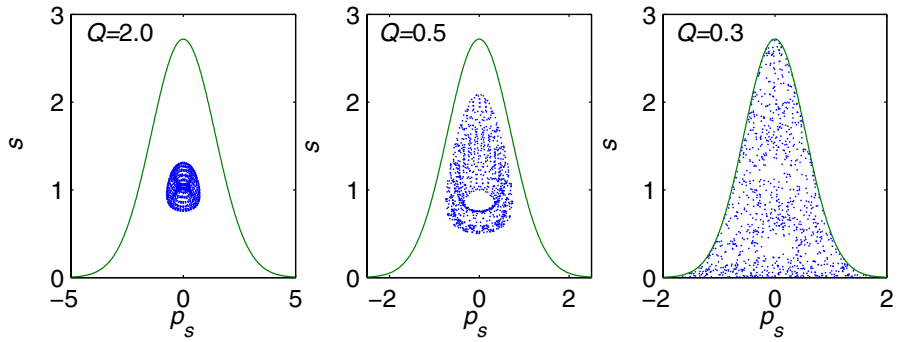

Figure 1. *Auxiliary variable phase-space with $Q = 2.0$, $Q = 0.5$, and $Q = 0.3$.*

provide a better understanding of the role of the Nosé mass parameter. We anticipate that a very similar analysis would apply to Nosé–Hoover dynamics.

2.1. Auxiliary variable phase-space. If we consider the classical N-body problem (2) with potential bounded below, $V(q) \geq 0 \ \ \forall q$ and apply a thermostat using the Nosé–Poincaré method (3), we can see that, for initial energy $E = H_0$,

$$\frac{p_s^2}{2Q} + N_f kT \ln s \leq E, \tag{4}$$

and hence the phase-space of the auxiliary variables is bounded by the equation

$$s = \exp\left(\frac{E - \frac{p_s^2}{2Q}}{N_f kT}\right). \tag{5}$$

We consider a harmonic oscillator with underlying energy $H(q,p) = p^2/2 + \omega^2 q^2/2$, thermostatted using the Nosé–Poincaré method, and examine, in Figure 1, the effect of a change in the Nosé mass on the auxiliary variable phase-space. The parameters used were $E = 1$, $kT = 1$ and $\omega = 1$ for $Q = 0.3$, $Q = 0.5$, and $Q = 2$. As Q is reduced the phase-space occupied by the auxiliary variables (dots) increases and the bounding curve (solid line), given by (5), decreases. At $Q \approx 0.3$ the auxiliary variables reach the boundary, and, at this point, although the system is not sufficiently ergodic to produce sampling from the canonical ensemble, the results are close in some sense as shown in Figure 2. From Nosé's linearized equation in [14], $Q = 2gkT/\omega^2$, where g is the number of degrees of freedom, we would expect that the optimum $Q = 2$, whereas in practice we see that at this value the system is sampling from the microcanonical ensemble.[1] Since the oscillator is started at the correct temperature we expect that the average value of s will be 1 (as shown in section 2.2).

In Figure 3 the relationship between the mean thermostat kinetic energy $\langle p_s^2/Q \rangle$ and Q is shown for Q in the range 0.001–2. $\langle p_s^2/Q \rangle$ peaks after the point where the auxiliary variables reach the boundary of their phase-space, as given in (5), at a value of approximately kT.

[1] In [10] introducing ergodicity by coupling a box of soft spheres into the thermostatting momentum resulted in the correct distributions, but only where $Q < NkT/(2\omega Q)$, corresponding to $Q < 0.5$ in the above example.

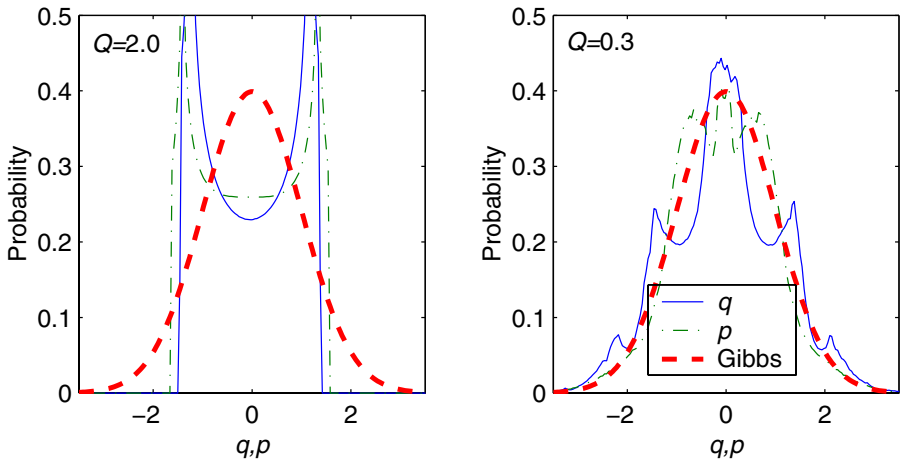

Figure 2. *Harmonic oscillator q, p distributions with $Q = 2$ and $Q = 0.3$.*

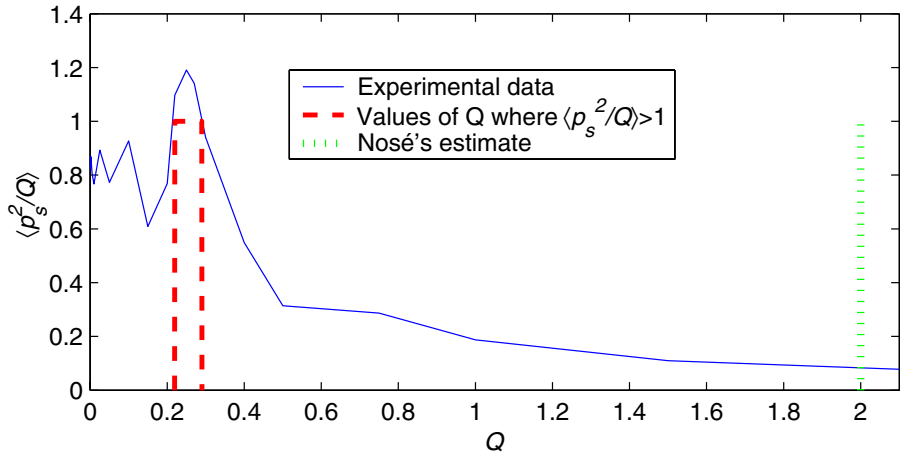

Figure 3. *$\langle p_s^2/Q \rangle$ for Q in the range 0.001–2 with values of Q for $\langle p_s^2/Q \rangle > 1$ (thick dashed) and Nosé's estimate (thick dots).*

2.2. Average values for the auxiliary variables. As shown in section 2.1, $\langle p_s^2/Q \rangle$ peaks at the optimum value for the Nosé mass Q. It is possible to calculate the average values for both the quantity p_s^2/Q and the auxiliary variable, s, if we assume that the system is ergodic. We consider the Nosé–Poincaré method (3), where it is possible to obtain real-time results without sacrificing the symplectic structure by using a Poincaré transformation.

Theorem 2.1. *When thermostatting systems of harmonic oscillators with the Nosé–Poincaré method* (3)*, if the system is ergodic, then the average of the auxiliary variable, s, will be given by*

$$\langle s \rangle = \exp\left(\frac{H_0}{N_f kT}\right)\left(\frac{N_f}{N_f+1}\right)^{\frac{2N_f+1}{2}}. \tag{6}$$

Proof. For an ergodic system the average of s is

$$\langle s \rangle = \frac{\int dp_s \int ds \int dp \int dq \; s \; \delta\left[H_{NP} - 0\right]}{\int dp_s \int ds \int dp \int dq \; \delta\left[H_{NP} - 0\right]} = \frac{\mathcal{N}}{\mathcal{D}}. \tag{7}$$

Substituting (3) into the numerator $\mathcal{N}$, of (7), we get

$$\mathcal{N} = \int dp_s \int ds \int dp \int dq \; s \; \delta\left[\left(H\left(q, \frac{p}{s}\right) + \frac{p_s^2}{2Q} + N_f kT \ln s - H_0\right) s\right]. \tag{8}$$

We can substitute $\tilde{p} = p/s$, and the volume element then becomes $dp = s^{N_f} d\tilde{p}$. There is no upper limit in momentum space, so we can change the order of integration of dp and ds, giving

$$\mathcal{N} = \int dp_s \int d\tilde{p} \int dq \int ds \; s^{N_f+1} \delta\left[\left(H(q, \tilde{p}) + \frac{p_s^2}{2Q} + N_f kT \ln s - H_0\right) s\right]. \tag{9}$$

Whenever a smooth function, $g(s)$, has a single simple root at $s = s_0$, we can write the equivalence relation for δ, $\delta[g(s)] = \delta[s - s_0]/|g'(s_0)|$; then

$$\begin{aligned} &\delta\left[\left(H(q, \tilde{p}) + \frac{p_s^2}{2Q} + N_f kT \ln s - H_0\right) s\right] \\ &= \frac{1}{N_f kT} \; \delta\left[s - \exp\left(-\frac{1}{N_f kT}\left(H(q, \tilde{p}) + \frac{p_s^2}{2Q} - H_0\right)\right)\right]. \end{aligned} \tag{10}$$

Substituting (10) into (9) and using the sifting property of δ, we get

$$\mathcal{N} = \frac{1}{N_f kT} \int dp_s \int d\tilde{p} \int dq \; \exp\left(-\frac{N_f + 1}{N_f kT}\left(H(q, \tilde{p}) + \frac{p_s^2}{2Q} - H_0\right)\right). \tag{11}$$

Due to the quadratic nature of the Hamiltonian for systems of harmonic oscillators, we can rescale $\hat{p} = \tilde{p} \; \sqrt{N_f + 1}$, $\hat{q} = q \; \sqrt{N_f + 1}$ and $\hat{p_s} = p_s \; \sqrt{N_f + 1}$ in (11),

$$\mathcal{N} = C_1 \int d\hat{p_s} \int d\hat{p} \int d\hat{q} \; \exp\left(-\frac{1}{N_f kT}\left(H(\hat{q}, \hat{p}) + \frac{\hat{p_s}^2}{2Q}\right)\right), \tag{12}$$

where

$$C_1 = \frac{1}{(N_f + 1)^{\frac{2N_f+1}{2}} N_f kT} \exp\left(\frac{(N_f + 1)H_0}{N_f kT}\right).$$

Similarly, we can substitute $\tilde{p} = p/s$ into the denominator, $\mathcal{D}$, of (7), use the equivalence relation for δ, and define $\bar{p} = \tilde{p} \; \sqrt{N_f}$, $\bar{q} = q \; \sqrt{N_f}$, and $\bar{p_s} = p_s \; \sqrt{N_f}$ to get

$$\mathcal{D} = C_2 \int d\bar{p_s} \int d\bar{p} \int d\bar{q} \; \exp\left(-\frac{1}{N_f kT}\left(H(\bar{q}, \bar{p}) + \frac{\bar{p_s}^2}{2Q}\right)\right), \tag{13}$$

where

$$C_2 = \frac{1}{N_f^{\frac{2N_f+1}{2}} N_f kT} \exp\left(\frac{N_f H_0}{N_f kT}\right).$$

Substituting (12) and (13) into (7), we get (6) as required. ■

We note that $\exp(x) = \lim_{n\to\infty}(1 + x/n)^n$. Then, in the limit $N_f \to \infty$,

$$\langle s\rangle = \exp\left(\frac{H_0}{N_f kT} - 1\right). \tag{14}$$

Substituting $N_f = 1$ into (6) gives $\langle s\rangle = \exp(H_0/kT - 1.04)$, a result close to (14). From this we conclude that (14) is a good approximation of $\langle s\rangle$ for all N_f.

We also have the following theorem.

Theorem 2.2. *When thermostatting with the Nosé–Poncaré method* (3)*, if the system is ergodic, then the average of the quantity* p_s^2/Q *will be given by*

$$\left\langle \frac{p_s^2}{Q}\right\rangle = kT. \tag{15}$$

Proof. If the system is ergodic, then the average of p_s^2/Q will be given by substituting p_s^2/Q for s in (7). In a method similar to that used above, we can substitute $\tilde{p} = p/s$ and use the equivalence relation for δ in both the denominator and numerator of the new equation. Noting that

$$\int_{-\infty}^{\infty} \frac{p_s^2}{Q} \exp\left(-\frac{p_s^2}{2QkT}\right) dp_s = kT \int_{-\infty}^{\infty} \exp\left(-\frac{p_s^2}{2QkT}\right) dp_s, \tag{16}$$

the new equation reduces to (15). ■

2.3. Frequency domain model of the Nosé–Poincaré method. We would like to analyze Nosé's method to determine the optimum value of Q, but, despite its apparent simplicity, Nosé's method is difficult to analyze dynamically. An alternative approach is to model the method in the frequency domain, and to do this it is necessary to use a method where the dynamics are in real time such as the Nosé–Poincaré method. By modeling the system for Q greater than its "optimum value," the value of Q at which the auxiliary variables intersect the boundary of their phase-space can be determined.

Consider a system with a Hamiltonian,

$$H_N(q,p) = \frac{p^2}{2m} + \frac{q^2}{2}. \tag{17}$$

The corresponding Nosé–Poincaré Hamiltonian is given by (3). We will assume that the fundamental frequency of the modified system is unchanged at $\omega = m^{-\frac{1}{2}}$ and that all other frequencies in p/s and q are of sufficiently small magnitude to be ignored. In addition, we will assume that time averages of time derivatives vanish, i.e., for $x(t)$ and time $\mathbb{T}$,

$$\langle \dot{x}(t)\rangle = \lim_{\mathbb{T}\to\infty} \frac{1}{\mathbb{T}} \int_0^{\mathbb{T}} \dot{x}(t)\, dt = \lim_{\mathbb{T}\to\infty} \left(\frac{x(\mathbb{T}) - x(0)}{\mathbb{T}}\right) = 0. \tag{18}$$

We can determine the average value of the oscillator kinetic term by considering the equations of motion for p_s,

$$\dot{p}_s = -\frac{\partial H_{NP}}{\partial s} = \frac{\tilde{p}^2}{m} - kT, \tag{19}$$

where $\tilde{p} = p/s$. Taking averages and using our second assumption gives

$$\left\langle \frac{\tilde{p}^2}{m} \right\rangle = kT. \tag{20}$$

These assumptions, and the predicted average kinetic energy, are generally observed in experiments.

We consider a harmonic oscillation and study the corresponding driven dynamics of the s, p_s variables. A harmonic vibration with average kinetic energy kT and frequency ω takes the form

$$\tilde{p} = \sqrt{2mkT}\cos(\omega t). \tag{21}$$

From the equation of motion for q,

$$\dot{q} = -\frac{\partial H_{NP}}{\partial p} = \frac{sp}{ms^2} = \frac{\tilde{p}}{m}, \tag{22}$$

we get

$$q = \sqrt{2kT}\sin(\omega t), \tag{23}$$

the constant of integration being zero for the harmonic oscillator.

These equations, together with the equations of motion, can then be used to solve for p_s and s. From the equations of motion for p_s,

$$\dot{p}_s = -\frac{\partial H_{NP}}{\partial s} = \frac{\tilde{p}^2}{m} - kT = \frac{2mkT\cos^2(\omega t)}{m} - kT = kT\cos(2\omega t), \tag{24}$$

integrating with respect to t,

$$p_s = \int kT\cos(2\omega t)\ dt = \frac{kT\sin(2\omega t)}{2\omega} + C_1, \tag{25}$$

where C_1 is a constant, which can be determined as follows. From the equations of motion for s,

$$\dot{s} = \frac{\partial H_{NP}}{\partial p_s} = \frac{sp_s}{Q}, \tag{26}$$

which can be rearranged as

$$\frac{Q\dot{s}}{s} = p_s. \tag{27}$$

From this we can see that p_s is a time derivative and has an average of zero,

$$\langle p_s \rangle = \left\langle \frac{Q\dot{s}}{s} \right\rangle = Q \left\langle \frac{d \ln s}{dt} \right\rangle = 0, \tag{28}$$

from our second assumption. Hence $C_1 = 0$, giving

$$p_s = \frac{kT \sin(2\omega t)}{2\omega}. \tag{29}$$

To obtain an expression for s we integrate both sides of (27) with respect to t to get

$$Q \ln s = -\frac{kT \cos(2\omega t)}{4\omega^2} + C_2 \tag{30}$$

for constant C_2. Hence,

$$s = C_3 \exp\left(-\frac{kT \cos(2\omega t)}{4Q\omega^2} \right), \tag{31}$$

where C_3 is a constant such that $\langle s \rangle$ satisfies (14). We can then show that

$$s = A \exp\left(\frac{H_0}{kT} - 1 \right) \exp\left(-\frac{kT \cos(2\omega t)}{4Q\omega^2} \right), \tag{32}$$

where

$$A = \left\langle \exp\left(-\frac{kT \cos(2\omega t)}{4Q\omega^2} \right) \right\rangle^{-1}. \tag{33}$$

There is strong experimental evidence in support of this model when Q is greater than its optimum value. Figure 4 shows the Fourier analysis of a harmonic oscillator, with $kT = 1$, $\omega = 1$, and $Q = 2$ for $\tilde{p}$ and p_s. We note that $\tilde{p}$ has a fundamental frequency of 0.167Hz, shifted slightly from the expected 0.159Hz by coupling with the thermostat, and p_s has a fundamental frequency (at the first harmonic) of 0.334Hz as predicted by the model.

If we consider the quantity

$$\langle |p_s| \rangle = \left\langle \left| \frac{kT \sin(2\omega t)}{2\omega} \right| \right\rangle = \frac{\sqrt{2} kT}{4\omega}, \tag{34}$$

we get the results in Table 1 for simulations of 2 million steps of 0.02, which again shows good correlation with the predicted results.

2.4. Estimating the Nosé mass. The model can be used to estimate the Nosé mass by calculating where the phase-space area occupied by the auxiliary variables interacts with the phase-space boundary, as shown in section 2.1. However, the straightforward application of the model gives too small a value for Q since it assumes a constant amplitude for the momentum satisfying the average kinetic energy equation (20), which is only one possible solution. In practice we see that the amplitude varies; indeed, this is a requirement if we are to obtain the correct sampling as we should sample the entire phase-space for the real variables, and

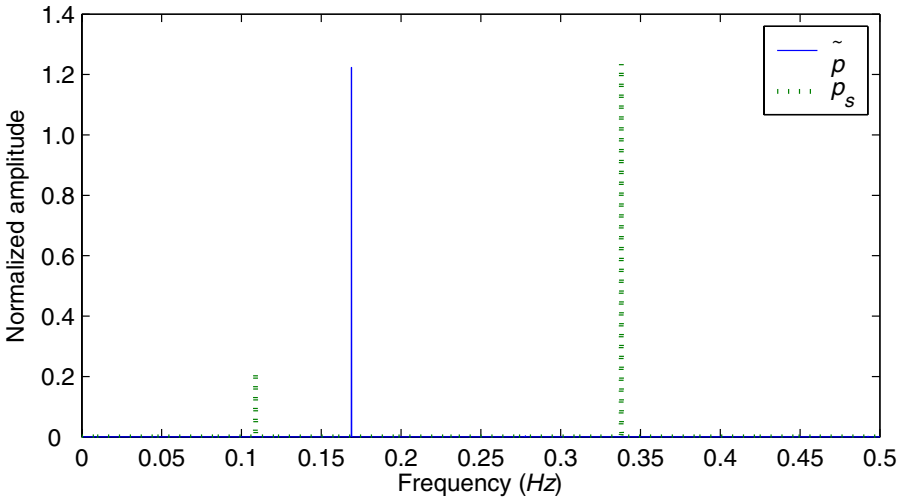

Figure 4. *Frequency domain plot with $Q = 2.0$. $\tilde{p}$ has a fundamental frequency of $0.167Hz$, and p_s has a fundamental frequency (at the first harmonic) of $0.334Hz$, as predicted in (29).*

Table 1
Average values for $|p_s|$ with varying Q and ω.

ω	Q	Actual $\langle\|p_s\|\rangle$	Model $\langle\|p_s\|\rangle$
1	.5	.349	.354
1	1	.361	.354
$\sqrt{2}$	1	.493	.501
$\sqrt{2}$	2	.510	.501

by estimating the maximum amplitude of p_s we can determine Q more accurately. Another source of error comes from the presence of additional small amplitude oscillations in p_s which are not predicted by the model but can be seen experimentally in Figure 4. This leads to an overestimation of Q which can be corrected by considering only the components of p_s which are consistent with the model—oscillations at the first harmonic of the thermostatted system.

We consider a modification to (29) where the variation in momentum leads to a real-valued function $a(t)$ which scales p_s such that

$$p_s = \frac{a(t)kT\sin(2\omega t)}{2\omega}. \tag{35}$$

For the purpose of finding the intersection of the region of phase-space occupied by the auxiliary variables and the phase-space boundary, we need only consider an envelope which contains the trajectory of the auxiliary variables. Examination of (29) and (32) shows that the requirements for the envelope are met by scaling (29) by $a = \max(a(t))$ and deriving the modified equation for s following the methods in section 2.3. This yields the equations for the scaled

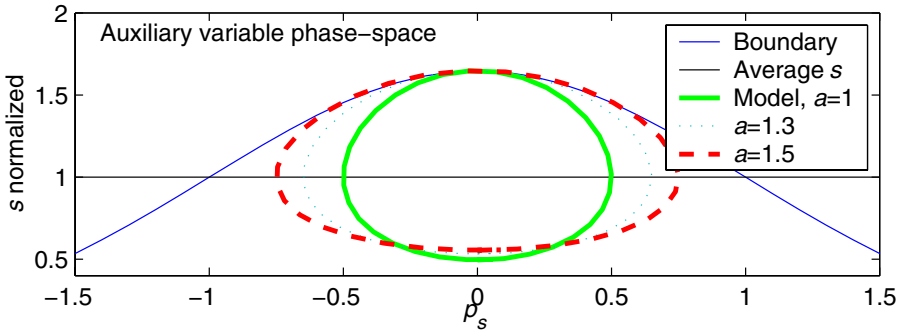

Figure 5. *Auxiliary variable phase-space for model scaling factors;* $a = 1$, $a = 1.3$, *and* $a = 1.5$, *where* s *is normalized,* $Q = 1$, *and* $kT = 1$.

auxiliary variables

$$p_s = \frac{akT\sin(2\omega t)}{2\omega} \tag{36}$$

and

$$s = A_{Q,a}\exp\left(\frac{H_0}{kT} - 1\right)\exp\left(-\frac{akT\cos(2\omega t)}{4Q\omega^2}\right), \tag{37}$$

where

$$A_{Q,a} = \left\langle \exp\left(-\frac{akT\cos(2\omega t)}{4Q\omega^2}\right)\right\rangle^{-1}. \tag{38}$$

While the phase-space occupied by the auxiliary variables does not interact with the boundary, some energy, say, E_r, is retained by the system at all times, and, from (5), the auxiliary variable phase-space is bounded by

$$\frac{p_s^2}{2Q} + kT\ln s = E - E_r. \tag{39}$$

From Figure 5, where the bounding curve is given by (39) for E_r defined at $a = 2$, we see that increasing the scaling factor a increases the maximum value of p_s, while $E - E_r$ in (39) is always defined by the maximum value of s. From this we expect a to be bounded above and $\max(a)$ can be estimated as follows.

Substituting (36) and (37) into (39),

$$\frac{a^2(kT)^2\sin^2(2\omega t)}{8Q\omega^2} + kT\ln A_{Q,a} + E - kT - \frac{a(kT)^2\cos(2\omega t)}{4Q\omega^2} = E - Er. \tag{40}$$

The $p_s^2/2Q$ term has maxima at $t = \pi/4\omega, 3\pi/4\omega, \ldots$, where the $\ln s$ term is at its average value and, conversely, the $\ln s$ term has maxima at $t = \pi/2\omega, 3\pi/2\omega, \ldots$, where $p_s^2/2Q = 0$.

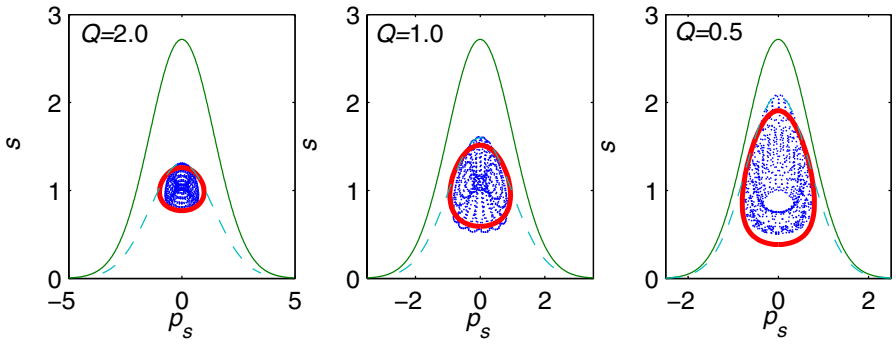

Figure 6. *Auxiliary variable phase-space with $Q = 2.0$, $Q = 1.0$, and $Q = 0.5$. Key: Actual phase-space=dots, predicted phase-space=thick solid, phase-space limit $E - E_r$=dashed, phase-space boundary=thin solid.*

The energy at the maxima for both $p_s^2/2Q$ and $\ln s$ is equal on the phase-space boundary from (40), allowing us to solve for a. Substituting $t = \pi/4\omega$ and $t = \pi/2\omega$ into (40) and equating the results to find $\hat{a} = \max(a)$,

$$\frac{\hat{a}^2(kT)^2}{8Q\omega^2} = \frac{\hat{a}(kT)^2}{4Q\omega^2}, \tag{41}$$

with nontrivial solution

$$\max(a) = \hat{a} = 2. \tag{42}$$

By examining Figure 6 we see that the value of E_r given by the model when $a = 2$ is correct, exactly enclosing the upper section of sampled auxiliary variable phase-space, and provides an upper bound for a. However, examination of the auxiliary variable phase-space trajectories for the model when $a = 2$ shows that for most of the trajectory the total energy would be greater than $E - E_r$, contravening (39). This discrepancy is related to the presence of different oscillations with small amplitude in both p_s and $\ln s$, as seen in Figure 4. An estimate for the upper bound when considering only the oscillations at the first harmonic, predicted by the model, can be found by solving for trajectories with energy not exceeding $E - E_r$, where E_r is defined when $a = 2$. Differentiating (40) with respect to t to find maxima,

$$\frac{a^2(kT)^2\sin(2\omega t)\cos(2\omega t)}{2Q\omega} + \frac{a(kT)^2\sin(2\omega t)}{2Q\omega} = 0, \tag{43}$$

giving maxima at $t = \pi/2\omega, 2\pi/\omega, \ldots$ and $\cos(2\omega t) = -a^{-1}$. Substituting $\cos(2\omega t) = -a^{-1}$ into (40) for the revised $\max(a)$, $\bar{a}$, gives

$$\frac{(\bar{a}^2 - 1)(kT)^2}{8Q\omega^2} + kT\ln A_{Q,\bar{a}} + E - kT + \frac{(kT)^2}{4Q\omega^2} = E - E_r. \tag{44}$$

For this to be within the energy bound imposed by $a = 2$, we have

$$\frac{(\bar{a}^2 - 1)(kT)^2}{8Q\omega^2} + \frac{(kT)^2}{4Q\omega^2} + kT\ln A_{Q,\bar{a}} = \frac{(kT)^2}{2Q\omega^2} + kT\ln A_{Q,2}, \tag{45}$$

where $A_{Q,2}$ is $A_{Q,a}$ defined at $a = 2$, with solution, when $\ln A_{Q,\bar{a}} \approx \ln A_{Q,2}$,

$$\bar{a} \approx \sqrt{3} \approx 1.73. \tag{46}$$

This result provides the maximum value for a when $\ln s$ is equal to $\langle \ln s \rangle$ and, for large Q, is close to $\ln \langle s \rangle$, the point at which we require the maximum value for p_s. For smaller Q we need to correct for variations in the $\ln A_{Q,a}$ term, which is dependent on Q. From (39) for the revised $\max(a)$, $\tilde{a}$, assuming (46) is correct for large Q,

$$\frac{\tilde{a}^2 (kT)^2}{8Q\omega^2} = \frac{3(kT)^2}{8Q\omega^2} + kT \ln A_{Q,\tilde{a}}, \tag{47}$$

giving

$$\tilde{a} = \sqrt{3 + \frac{8Q\omega^2 \ln A_{Q,\tilde{a}}}{kT}}. \tag{48}$$

For $Q = 0.5$, $kT = 1$, and $\omega = 1$ we get $\tilde{a} \approx 1.54$.

Figure 6 shows the experimental results for a thermostatted harmonic oscillator where $kT = 1$, $\omega = 1$, and $Q = 0.5, 1.0, 2.0$; the actual measurements are the dots, the predicted phase-space is the thick solid line, the phase-space limit $E - E_r$ is the dashed line, and the phase-space boundary is the thin solid line. This indicates that there is good correlation between the results predicted from the model and the actual experiments.

The maximum value of p_s from (46) and (36) is

$$\max(p_s) \le \frac{\bar{a} kT}{2\omega} \approx \frac{0.87kT}{\omega}. \tag{49}$$

Since the auxiliary variable's phase-space is bounded by (5), substituting the average value of s, given by (14), has solutions for p_s^*, the value of p_s at the phase-space boundary,

$$p_s^* = \sqrt{2QkT}, \tag{50}$$

for the single harmonic oscillator ($N = 1$). The auxiliary variables will reach the boundary of phase-space when $\max p_s = p_s^*$ from (50),

$$Q \le \frac{0.38kT}{\omega^2}. \tag{51}$$

This should be compared with Nosé's estimate in [14] of $Q = 2kT/\omega^2$. For the example of the harmonic oscillator, with $kT = 1$, $\omega = 1$, using the correction in (48), is $Q \approx 0.29$, which compares well with the experimentally obtained value of $Q = 0.3$ as shown in Figure 1.

2.5. Behavior of the Nosé–Poincaré method for small Q. For small values of Q it has been observed by Hoover [6] and others that the auxiliary variables will oscillate independently of the system to be thermostatted. Under these conditions, where the frequency of the system is less than that of the auxiliary variable self-oscillation frequency, Nosé's assumptions for the oscillation frequency now hold, as can be seen in Table 2 and Figure 7 for a thermostatted harmonic oscillator with $kT = 1$, $\omega = 1$. Experiments indicate that the onset of self-oscillation is typically around three times the fundamental frequency of the system, giving a very small band for the correct choice of Q, as seen in Figure 3. From this Figure we have $\langle p_s^2/Q \rangle \approx 0.8kT$ after the onset of self-oscillation, as Q decreases.

Table 2
Auxiliary variable self-oscillation frequency for small Q.

Q	$\sqrt{\frac{2gkT}{Q}}$ (Hz)	Actual (Hz)
0.005	3.3	2.8
0.01	2.3	2.0
0.02	1.7	1.4

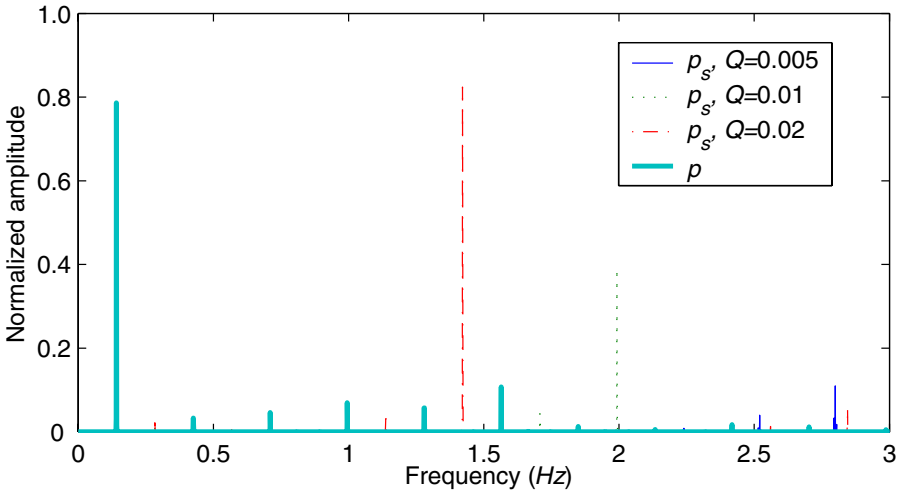

Figure 7. *Frequency domain plot of a Nosé–Poincaré thermostatted harmonic oscillator with $\omega = 1$ (0.167Hz) for small values of Q.*

2.6. Thermostatting multiple oscillators. The application of Nosé thermostats to multiple harmonic oscillators can be analyzed in a similar manner to the case of the single harmonic oscillator.

It is generally assumed that the auxiliary variables will only interact with parts of the thermostatted system which have a fundamental frequency near to the self-oscillation frequency of the auxiliary variables. This is not generally the case as can be seen from Figure 8, a Fourier plot of the auxiliary variable when thermostatting four oscillators of frequencies $\omega_1 = 1.00$, $\omega_2 = 0.308$, $\omega_3 = 0.095$, and $\omega_4 = 0.052$, temperature $kT = 1$, and Nosé mass $Q = 2gkT/\omega_4^2 = 3200$ (which should resonate with oscillator 4). The magnitude of the position components for each oscillator are approximately the same; from (21) the magnitude of the oscillator's momentum will be proportional to ω^{-1}, and from (29) the magnitude of the component for each oscillator in the auxiliary variable momentum, p_s, will be proportional to an additional ω^{-1}, and hence p_s has been scaled by ω^2. Note that, in this microcanonical experiment, each oscillator is represented by its first harmonic in the auxiliary variable momentum, as predicted in the model of section 2.3, and that the interaction with the auxiliary variables is similar for all of the oscillators.

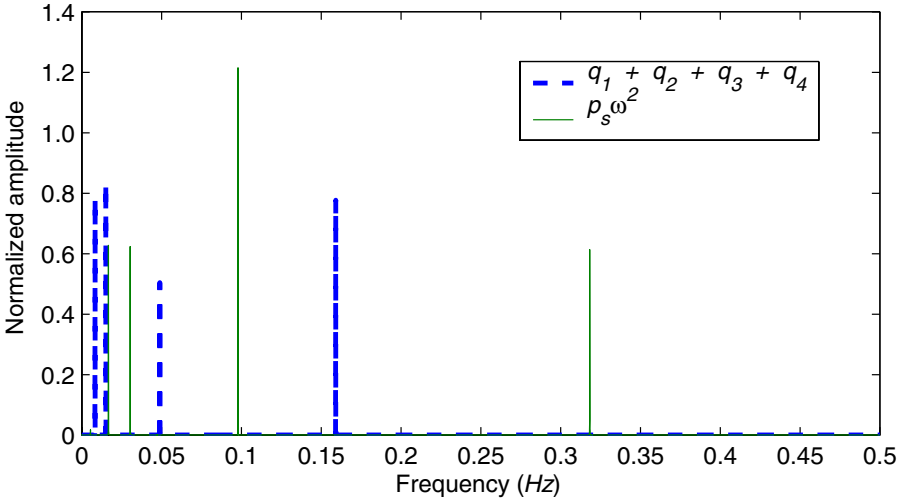

Figure 8. *Frequency domain plot of position and scaled auxiliary variable momentum for four oscillators.*

2.7. Extension of the model for multiple oscillators. The model of section 2.3 can easily be extended to multiple harmonic oscillators. Given a Hamiltonian for N oscillators,

$$\tilde{H}_N = \sum_{i=1}^{N} \left(\frac{p_i^2}{2m_i} + \frac{q_i^2}{2} \right). \tag{52}$$

The corresponding Nosé–Poincaré Hamiltonian is given in (3). As before we will assume that the fundamental frequencies of the modified system are the same as those in the original system and that all other frequencies are of sufficiently small magnitude to be ignored. In addition, we will assume that time averages of time derivatives vanish and that the initial energy is equally distributed between the oscillators. Then,

$$\left\langle \frac{\tilde{p}_i^{\,2}}{m_i} \right\rangle = kT, \tag{53}$$

where $\tilde{p}_i = p_i/s$. Following the analysis as before yields

$$\tilde{p}_i = \sqrt{2m_i kT}\cos(\omega_i t), \quad q_i = \sqrt{2kT}\sin(\omega_i t), \quad i = 1, 2, \ldots, N, \tag{54}$$

$$p_s = \sum_{i=1}^{N} \frac{kT\sin(2\omega_i t)}{2\omega_i}, \tag{55}$$

$$s = \tilde{A}\exp\left(\frac{H_0}{NkT} - 1\right) \prod_{i=1}^{N} \exp\left(-\frac{kT\cos(2\omega_i t)}{4Q\omega_i^2}\right), \tag{56}$$

where

$$\tilde{A} = \left\langle \prod_{i=1}^{N} \exp\left(-\frac{kT\cos(2\omega_i t)}{4Q\omega_i^2}\right)\right\rangle^{-1}. \tag{57}$$

To estimate the optimum Nosé mass for multiple oscillators, we can modify (49) using (54)–(56) to obtain

$$\max(p_s) = \max\left(a\sum_{i=1}^{N}\frac{kT\sin(2\omega_i t)}{2\omega_i}\right), \tag{58}$$

where $a \leq 2$ from (42). Solutions for p_s^*, p_s on the auxiliary variable phase-space bounding curve (5), when s is at an average value (14), are

$$p_s^* = \sqrt{2QN_f kT} \tag{59}$$

and will be the point where p_s is at its maximum. The optimum value for Q will occur when (58) and (59) are equal.

If we consider a system where all of the oscillators are of similar frequency, ω, and set $a = 2$, the upper bound for a, we have

$$\max(p_s) \leq \frac{N_f kT}{\omega}, \tag{60}$$

giving optimum Q,

$$Q \leq \frac{N_f kT}{2\omega^2}. \tag{61}$$

Compare this with Nosé's estimate $Q = 2N_f kT/\omega^2$. As before a more accurate estimate for a could be obtained, but this would only be useful for very specific cases as it is unlikely that all of the oscillators will be of exactly the same frequency. For mixed frequency systems the model (55)–(56) can be used to accurately predict the optimum value of Q, which was not previously possible using linearization methods.

However, if we compare the auxiliary variable phase-space for four harmonic oscillators of different frequencies with that of the single harmonic oscillator, we see that the area of phase-space used is similar in both examples; see Figure 9. This is expected as the probability of the entire system's energy residing in the auxiliary variables is small. In addition, it is shown in section 4 (78) that if the auxiliary variables were homogeneously distributed, then we would have $\langle p_s^2/Q\rangle = N_f kT$, which is contrary to both the results in section 2.2 and the values predicted by the equipartition theorem.

If we assume that there is no correlation between the dynamics of each body and the trajectories are random in relation to each other, then we can analyze this as follows. The auxiliary variable momentum p_s is driven by the variations in the kinetic energy of the system, as we can see from its equations of motion. As the dimension, N_f, of the system increases, the variations in kinetic energy will now be reduced by a factor $1/\sqrt{N_f}$, and hence the magnitude

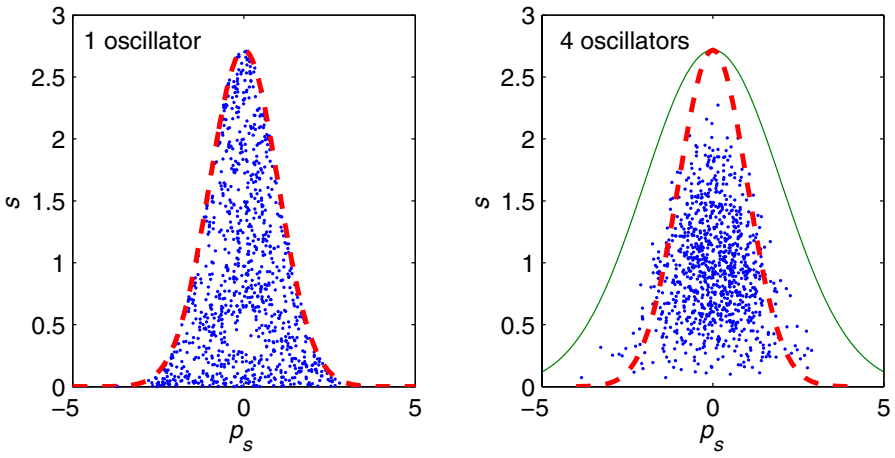

Figure 9. *Comparison of auxiliary variable phase-space for one and four oscillators. Key: Single oscillator phase-space boundary=thick dashed, four oscillator phase-space boundary=solid.*

of p_s will increase by $\sqrt{N_f}$ rather than by N_f as assumed in (60). If we substitute $\sqrt{N_f}\tilde{p}_s = p_s$ into (5), where $E = \tilde{H}_0$, we get

$$s = \exp\left(\frac{\tilde{H}_0}{N_f kT} - \frac{\tilde{p}_s^2}{2QkT}\right), \tag{62}$$

which coincides with both the auxiliary variable phase-space for the single harmonic oscillator and the results obtained experimentally as shown in Figure 9.

For the calculation of the Nosé mass we now have, for oscillators of similar frequency close to ω,

$$\max(\tilde{p}_s) = \frac{\sqrt{N_f}kT}{\omega}, \tag{63}$$

and a bound on $\tilde{p}_s$ at $\langle s \rangle$ of

$$\tilde{p}_s = \sqrt{2QkT}, \tag{64}$$

giving optimum $Q = N_f kT/2\omega^2$, which is the same as in (61). Experiments with four to eight oscillators indicate that using the masses predicted by Nosé's linearization method does not give sampling in the canonical ensemble, the onset of this behavior occurring close to the prediction of (61).

3. Multiple thermostat methods. In this section we develop the new recursive multiple thermostatting scheme and show that it samples from the canonical ensemble. We will actually show this for a more general formulation of momentum scaling methods from which the RMT method is derived.

Given a Hamiltonian system where $H(q,p)$ is the energy of an N-body system, $q = (q_1, q_2, \ldots, q_N)$ and $p = (p_1, p_2, \ldots, p_N)$ are the positions and momenta of the N bodies; a

generalized Hamiltonian formulation for this class of thermostat is given by

$$H_{GT}(q,p,s_1,s_2,\dots,p_{s_1},p_{s_2},\dots) = H\left(q,\frac{p}{s_{i_1}s_{i_2}\cdots}\right) + H_G(s_1,s_2,\dots,p_{s_1},p_{s_2},\dots), \tag{65}$$

where $s_1, s_2, \dots$ are the auxiliary variables, $p_{s_1}, p_{s_2}, \dots$ are the auxiliary variables momenta, $\{s_{i_1}, s_{i_2}, \dots\}$ is the set of auxiliary variables which scale the momenta of the original system, and H_G is the part of the revised Hamiltonian which dictates the dynamics of the auxiliary variables. Since rescaling the momentum also rescales time, it is appropriate to apply a time reparametrization in the revised system using either a Sundman (as in the Nosé–Hoover formulation [6]) or Poincaré transformation as in [2]. When there is no time rescaling, or when it is done using a Poincaré transformation, the resulting system has a Hamiltonian structure, and it is possible to show analytically that the modified system samples from the canonical ensemble subject to certain constraints. It is primarily these methods that will be considered here.

3.1. Multiple thermostats. It is possible to introduce additional thermostats into the Nosé and Nosé–Poincaré methods while retaining both their Hamiltonian structure and sampling from the canonical ensemble. This can be illustrated in a more general setting by rewriting the Nosé method, (1), to include the momenta of the thermostatting variable with the system momenta such that $\hat{p} = (p_1, p_2, \dots, p_N, p_{N+1})$ to give

$$\begin{aligned} H_N(q,s_1,\hat{p}) &= \hat{H}_N\left(q,\frac{p_1}{s_1},\frac{p_2}{s_1},\dots,\frac{p_N}{s_1},p_{N+1}\right) + (N_f+1)kT\ln s_1 \\ &= \hat{H}_N(q,\hat{p}') + (N_f+1)kT\ln s_1, \end{aligned}$$

where

$$\hat{H}_N(q,\hat{p}) = H\left(q,p_1,p_2,\dots,p_N\right) + \frac{p_{N+1}^2}{2Q_1}$$

and

$$\hat{p}' = \left(p_1',p_2',\dots,p_N',p_{N+1}'\right) = \left(\frac{p_1}{s_1},\frac{p_2}{s_1},\dots,\frac{p_N}{s_1},p_{N+1}\right). \tag{66}$$

A second thermostat can be added as follows:

$$\begin{aligned} H_{NT}(q,s_1,s_2,\hat{p},p_{N+2}) = \hat{H}_N &\left(q,p_{j_1}',\dots,p_{j_{N+1-M}}',\frac{p_{i_1}{}'}{s_2},\dots,\frac{p_{i_M}{}'}{s_2}\right) \\ &+(N_f+1)kT\ln s_1 + \frac{p_{N+2}^2}{2Q_2} + gkT\ln s_2 + f_2(s_2), \end{aligned}$$

where $f_2(s_2)$ is a real-valued function, g is a scalar, and the new thermostat is applied to M of the momenta, the thermostatted set being $\{p_{i_1}', \dots, p_{i_M}'\}$ and the nonthermostatted set being $\{p_{j_1}', \dots, p_{j_{N+1-M}}'\}$ for some integers $i_1, \dots, i_M$, $j_1, \dots, j_{N+1-M}$. Note that the thermostatted

set may include any of the system momenta and the thermostatting variable momenta. The partition function for this method, for energy E, is defined as

$$Z = \frac{1}{N!h^{N_f}} \int dp_{N+2} \int ds_2 \int ds_1 \int d\hat{p} \int dq \; \delta\left[H_{NT} - E\right], \tag{67}$$

where h is Planck's constant. We can substitute $p'_i = p_i/s_1, \quad 1 \le i \le N, \; p'_{N+1} = p_{N+1}$, and the volume element then becomes $d\hat{p} = s_1^{N_f} d\hat{p}'$, where $\hat{p}'$ is defined as above. There is no upper limit in momentum space, so we can change the order of integration of $d\hat{p}'$ and ds_1, giving

$$Z = \frac{1}{N!h^{N_f}} \int dp_{N+2} \int ds_2 \int d\hat{p}' \int dq \int ds_1 \; s_1^{N_f} \delta\left[H_{NT} - E\right].$$

Using the equivalence relation for δ, $\delta[g(x)] = \delta[x-x_0]/|g'(x)|$, where x_0 is the zero of $g(x) = 0$, for $x = s_1$, and noting that $s_1 > 0$ is assumed as a natural consequence of the form of the Hamiltonian, we get

$$\begin{aligned} Z = & \frac{1}{N!h^{N_f}(N_f+1)kT} \int dp_{N+2} \int ds_2 \int d\hat{p}' \\ & \times \int dq \; \exp\left(\frac{-\left(\hat{H}_N + \frac{p_{N+2}^2}{2Q_2} + gkT\ln s_2 + f_2(s_2) - E\right)}{kT} \right). \end{aligned}$$

We can substitute $p''_l = p'_l/s_2, \quad l \in \{i_1, \ldots, i_M\}, \; p''_l = p'_l, \quad l \in \{j_1, \ldots, j_{N+1-M}\}$, and the volume element then becomes $d\hat{p}' = s_2^M d\hat{p}''$, where $\hat{p}'' = (p''_1, p''_2, \ldots, p''_{N+1})$. There is no upper limit in momentum space, so we can change the order of integration of $d\hat{p}''$ and ds_2, giving

$$\begin{aligned} Z = & \frac{1}{N!h^{N_f}(N_f+1)kT} \int dp_{N+2} \int d\hat{p}'' \int dq \\ & \times \int ds_2 \; s_2^M \exp\left(\frac{-\left(\hat{H}_N(q,\hat{p}'') + \frac{p_{N+2}^2}{2Q_2} + gkT\ln s_2 + f_2(s_2) - E\right)}{kT} \right), \\ = & \frac{1}{N!h^{N_f}(N_f+1)kT} \int dp_{N+2} \int d\hat{p}'' \int dq \int ds_2 \; s_2^{M-g} \exp\left(\frac{-f_2(s_2)}{kT} \right) \\ & \times \exp\left(\frac{-\left(\hat{H}_N(q,\hat{p}'') + \frac{p_{N+2}^2}{2Q_2} - E\right)}{kT} \right). \end{aligned}$$

If we choose $g = M$ and suppose that

$$\int_0^\infty \exp\left(\frac{-f_2(x)}{kT} \right) \; dx = K_2 < \infty,$$

then

$$Z = \frac{K_2}{N! h^{N_f} (N_f + 1) kT} \int dp_{N+2} \int d\hat{p}'' \int dq \ \exp\left(\frac{-\left(\hat{H}_N(q, \hat{p}'') + \frac{p_{N+2}^2}{2Q_2} - E \right)}{kT} \right).$$

Integrating over both thermostat momenta, p''_{N+1} and p_{N+2}, gives

$$Z = \frac{C}{N! h^{N_f}} \int dp'' \int dq \ \exp\left(\frac{-H(q, p'')}{kT} \right),$$

where

$$C = \frac{2\pi K_2 \sqrt{Q_1 Q_2}}{N_f + 1} \ \exp\left(\frac{E}{kT} \right)$$

and

$$p'' = (p''_1, p''_2, \ldots, p''_N).$$

This process can be repeated to add more thermostats, with the possibility at each stage of thermostatting the previous thermostat's momentum in addition to any of the other momenta. A similar proof can be applied to the Nosé–Poincaré method.

3.2. Multiple thermostat schemes. The general Hamiltonian for this class of methods, with M thermostats, will then be

$$H_{NM} = \sum_{j=1}^{N} \frac{p_j^2}{2 m_j s_{k_1}^2 s_{k_2}^2 \cdots s_{k_m}^2} + V(q) + \sum_{i=1}^{M-1} \frac{p_{s_i}^2}{2 Q_i \psi_i} + \frac{p_{s_M}^2}{2 Q_M}$$
$$+ g kT \ln s_1 + \sum_{i=2}^{M} (g_i kT \ln s_i + f_i(s_i)), \tag{68}$$

where $g = N_f + 1$. The original system is thermostatted by a subset of the thermostats, $\{s_{k_1}, s_{k_2}, \ldots, s_{k_m}\}$, with $\{k_1, k_2, \ldots, k_m\} \subseteq \{1, 2, \ldots, M\}$. The ith thermostat is thermostatted by ψ_i, defined as

$$\psi_i = \prod_{j=1}^{n_i} s_{l_j}^2,$$

where $\{l_1, l_2, \ldots, l_{n_i}\} \subseteq \{i+1, i+2, \ldots, M\}$. g_i is the number of degrees of freedom thermostatted by the ith thermostat, and the auxiliary functions, $\{f_i(s_i)\}$, are real valued, satisfying

$$\int_0^\infty \exp\left(\frac{-f_i(x)}{kT} \right) \ dx = K_i < \infty. \tag{69}$$

Remark. The Nosé–Poincaré variation can be produced by applying a Poincaré time transformation to (68) using a time reparametrization variable equal to $s_{k_1} s_{k_2} \cdots s_{k_m}$ and setting $g = N_f$.

3.3. Nosé–Poincaré chains. Nosé–Poincaré chains can be derived from (68) as

$$H_{NPC} = s_1 \left[H\left(q, \frac{p}{s_1}\right) + \sum_{i=1}^{M-1} \frac{p_{s_i}^2}{2Q_i s_{i+1}^2} + \frac{p_{s_M}^2}{2Q_M} + N_f kT \ln s_1 + \sum_{i=2}^{M} (kT \ln s_i + f_i(s_i)) - H_0 \right], \tag{70}$$

where the auxiliary functions $\{f_i(s_i)\}$ are real-valued and satisfy (69) and H_0 is chosen such that $H_{NPC} = 0$ when evaluated at the initial conditions.

As discussed in section 1, the stability of the numerical implementation of chains is not as good as the underlying Nosé–Poincaré method, and the low dimension of the subsystem to be thermostatted by each new thermostat means that the expected average value of $p_{s_i}^2/(Q_i s_{i+1}^2)$ may not be easily achievable, as demonstrated by the results in Table 3. To overcome these deficiencies while retaining the insensitivity to the values of the Nosé masses requires a new approach to the problem.

3.4. Recursive Nosé/Nosé–Poincaré thermostats. An alternative approach is to apply a Nosé thermostat to the original Hamiltonian and then apply a second thermostat to all of the "kinetic" terms in the new Hamiltonian, including the term for p_{s_1}, the thermostatting variable momentum. This method can then be applied recursively to add as many thermostats as required with the dimension of the system to be thermostatted increasing for each thermostat. This leads to better stability when compared with chains, as the time reparametrization involves all of the thermostats and generally requires only one additional thermostat even for low dimensional systems. The Hamiltonian for the formulation without time rescaling, with M thermostats, will be

$$H_{NR} = \sum_{j=1}^{N} \frac{p_j^2}{2m_j s_1^2 s_2^2 \cdots s_M^2} + V(q) + \sum_{i=1}^{M-1} \frac{p_{s_i}^2}{2Q_i s_{i+1}^2 \cdots s_M^2} + \frac{p_{s_M}^2}{2Q_M} + gkT \ln s_1 + \sum_{i=2}^{M} ((N_f + i - 1)kT \ln s_i + f_i(s_i)), \tag{71}$$

where $g = N_f + 1$ and the auxiliary functions, $\{f_i(s_i)\}$, are real-valued satisfying equation (69).

The Nosé–Poincaré method is derived from this by applying a rescaling of time by $s_1 s_2, \ldots s_M$,

$$H_{NPR} = s_1 s_2 \cdots s_M \left[H_{NR} - H_0 \right], \tag{72}$$

where H_0 is chosen such that $H_{NPR} = 0$ at initial conditions and setting $g = N_f$.

3.5. Choice of the auxiliary function. For the additional thermostats to work correctly, an auxiliary function, $f_i(s_i)$, must be chosen not only to satisfy (69) but also to provide a suitable modification to the thermostats. One such choice is

$$f_i(s_i) = \frac{(a_i - s_i)^2}{2C_i}, \tag{73}$$

where C_i, the auxiliary function coefficient, is a constant. The value a_i is chosen as the required average value of s_i, generally 1, as the additional term will operate as a negative feedback loop to minimize $(a_i - s_i)$, as can be seen from the equations of motion. For a Hamiltonian as given in (2), the equations of motion for p_{s_i} and s_i in the equivalent Nosé chain system will be

$$\dot{p}_{s_i} = \frac{p_{s_{i-1}}}{Q_{i-1}s_i^3} - \frac{kT}{s_i} + \frac{(a_i - s_i)}{C_i}, \quad \dot{s}_i = \frac{p_{s_i}}{Q_i s_{i+1}^2}. \tag{74}$$

Assuming C_i is sufficiently small, if s_i increases above a_i, then p_{s_i} will decrease, eventually decreasing s_i. Conversely, if s_i decreases below a_i, then p_{s_i} will increase, eventually increasing s_i.

In the context of Nosé–Poincaré chains, the value of C_i, $i \geq 2$, can be estimated by considering the equations of motion for the ith thermostat (74). From this we see that s_i is driven by the changes in $p_{s_{i-1}}$. The purpose of the auxiliary function is to limit the excursions of s_i, which can be achieved if $ds_i/dp_{s_{i-1}}$ is a maximum at $s_i = a_i$. From this it was shown in [12] that C_i should satisfy

$$C_i \leq \frac{a_i^2}{8kT}. \tag{75}$$

4. Analysis of multiple thermostat schemes. With the introduction of multiple thermostats it is now possible to have multiple Nosé masses. From the analysis in section 2, we can see that a good choice of masses occurs where the auxiliary variables approach their phase-space boundary and expected averages. From this we conclude that the introduction of multiple thermostats can be used to enforce the ergodicity of the system.

4.1. Expected average values for p_s^2/Q. If we consider the single harmonic oscillator thermostatted by the Nosé–Poincaré method, from (36) and (37) we would expect the maximum value of p_s to occur when s is at its average value, where the phase-space boundary for p_s is given by (50) as $\sqrt{2QkT}$. This, together with the observation from (36) that $\max\left(p_s^2\right) = 2\left\langle p_s^2 \right\rangle$, gives

$$\left\langle \frac{p_s^2}{Q} \right\rangle = kT. \tag{76}$$

From this we observe that the average value of p_s^2/Q, when Q is greater than the "optimum" value, is always less than kT, which is observed in practice and illustrated in Figure 3.

If the phase-space trajectories of the auxiliary variables were homogenously distributed, we could calculate the average value from the auxiliary variable phase-space using (5). Here the probability density function for p_s would be

$$\rho_{p_s} = \frac{\exp\left(-\frac{p_s^2}{2QNkT}\right)}{\int_{-\infty}^{\infty} \exp\left(-\frac{p_s^2}{2QNkT}\right) dp_s}, \tag{77}$$

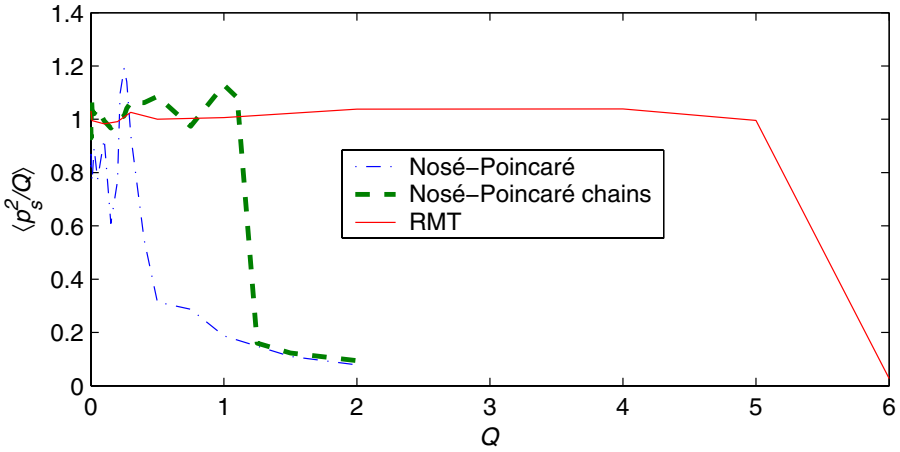

Figure 10. $\langle p_s^2/Q \rangle$ *for* Q *in the range* 0.001-6.

and then

$$\left\langle \frac{p_s^2}{Q} \right\rangle = \int_{-\infty}^{\infty} \frac{p_s^2}{Q} \rho_{p_s} dp_s = NkT. \tag{78}$$

For the single harmonic oscillator, where $N = 1$, this would give the same result as (15) but would raise some interesting questions for multiple oscillators.

4.2. Obtaining expected average values independently of Q. From Figure 3 it is clear that the correct choice of Q is limited to a very narrow band, but from the discussion above another possibility presents itself—that of thermostatting the thermostat to ensure that $\langle p_s^2/Q \rangle = kT$. A variation of this, Nosé–Hoover chains, was first proposed by Martyna, Klein, and Tuckerman in [13] and was seen as providing additional ergodicity to the system so that the modified system sampled from the canonical ensemble. In [13] it was shown that the single harmonic oscillator could be successfully thermostatted by this method. In Figure 10, $\langle p_s^2/Q \rangle$ is plotted against Q for a Nosé–Poincaré chains integrator consisting of five thermostats with $Q_j = 2Q$ and $C_j = 0.08$, where $kT = 1$. From this we see that the range of Q is increased and that chains can also limit the activity of the auxiliary variables, preventing them from entering self-oscillation.

As discussed in section 3.3, the required average value of $p_{s_i}^2/(Q_i s_{i+1}^2)$ for each thermostat may not be achievable. If we consider the Nosé–Poincaré chains Hamiltonian (70), the average values for $p_{s_i}^2/(Q s_{i+1}^2)$ can be obtained, if the system is ergodic, by substituting $p_{s_i}^2/(Q s_{i+1}^2)$ for s in (7). In a method similar to that used in section 2.2, we can substitute $\tilde{p}_{s_i} = p_{s_i}/s_{i+1}$ and use the equivalence relation for δ in both the denominator and numerator of the new equation. Noting that

$$\int_{-\infty}^{\infty} \frac{s_j}{a_j} \exp\left(-\frac{(a_j - s_j)^2}{C_j}\right) ds_j \approx \int_{-\infty}^{\infty} \exp\left(-\frac{(a_j - s_j)^2}{C_j}\right) ds_j \tag{79}$$

Table 3

Average values for $\frac{p_{s_i}^2}{Q_i s_{i+1}^2}$ *using chains and recursive methods.*

i	Chains $\left\langle \frac{p_{s_i}^2}{Q_i s_{i+1}^2} \right\rangle$	Recursive $\left\langle \frac{p_{s_i}^2}{Q_i s_{i+1}^2} \right\rangle$	Predicted
1	0.987	1.000	1.000
2	0.678	0.973	1.000
3	0.543	N/A	1.000
4	0.484	N/A	1.000
5	0.525	N/A	1.000

and that

$$\int_{-\infty}^{\infty} \frac{\tilde{p}_{s_i}^2}{Q_i} \exp\left(-\frac{\tilde{p}_{s_i}^2}{2Q_i kT}\right) dp_{s_i} = kT \int_{-\infty}^{\infty} \exp\left(-\frac{\tilde{p}_{s_i}^2}{2Q_i kT}\right) dp_{s_i}, \tag{80}$$

the new equation reduces to

$$\left\langle \frac{p_{s_i}^2}{Q_i s_{i+1}^2} \right\rangle = kT. \tag{81}$$

Similarly, we can show

$$\left\langle \frac{p_{s_M}^2}{Q_M} \right\rangle = kT. \tag{82}$$

A Nosé–Poincaré chains integrator consisting of five thermostats with $Q_i = 2Q$ and $C_j = 0.08$, where $kT = 1$, integrated over 20,000,000 steps of 0.01 gave the averages in Table 3. Even if the dimension of the underlying system is increased, this problem persists; hence the system is not ergodic, and the proof of sampling from the canonical ensemble is invalid.

An alternative solution is to use recursive thermostatting (71) and (72), introduced in section 3.4, where the complete system, including the preceding thermostat, is thermostatted. This means that each new thermostat will thermostat a system of increasing dimension, and where the underlying system is large, sampling will be close to the canonical ensemble. It has been found that, even for low dimensional systems, one additional thermostat is usually sufficient to provide good sampling. As discussed in section 3.3, stability is also increased when compared to chains, allowing larger step sizes. In Figure 10 we see that the range of possible values for Q is vastly increased, and the average value of $p_{s_i}^2/(Q_i s_{i+1}^2)$ is closer to 1, when compared to the Nosé–Poincaré chains method, as seen in Table 3.[2]

[2] *Remark.* Fast thermostatting can be accomplished by use of the RMT scheme. In traditional thermostatting schemes the optimum value for Q, from (61), increases with the dimension of the system resulting in a dramatic increase in thermostat response time for large systems, which may be undesirable. From Figure 10 we see that thermostatting the thermostat gives a vastly increased range for Q which allows very small values to be used, giving a much faster response.

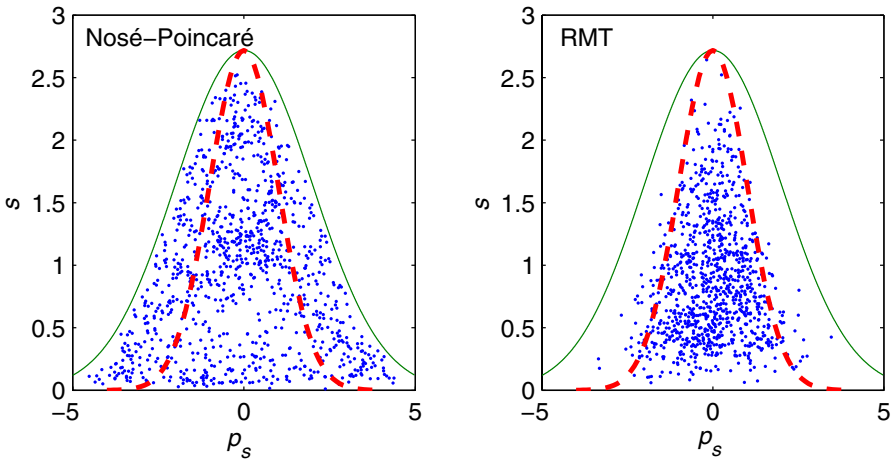

Figure 11. *Auxiliary variable phase-space for four oscillators of similar frequency for the Nosé–Poincaré and RMT methods. The dashed line is the single oscillator phase-space boundary, and the solid line is the four oscillator phase-space boundary.*

4.3. Obtaining expected average values independently of Q for multiple oscillators.

In section 4 we saw that $\langle p_s^2/Q \rangle = kT$, based on the model in section 2.3, was sufficient for the auxiliary variables to interact with their phase-space boundary for a single harmonic oscillator, giving rise to the behavior required to sample from the canonical ensemble. In section 2.7 it was shown that the volume of auxiliary variable phase-space sampled by the system is essentially independent of the number of oscillators being considered, despite the increase in the available volume from (5), if the system is ergodic. From this we would expect that thermostatting the thermostat to ensure that $\langle p_s^2/Q \rangle = kT$ would give good results for multiple oscillators, with a much reduced dependence on Q, as we saw for the case of the single harmonic oscillator, and this can be seen in experiments. However, there may be additional benefits for multiple oscillators, and these can be classified for systems consisting of oscillators of similar frequency and multiscale systems.

4.3.1. Multiple oscillators of similar frequency. The boundary derived in section 2.7 assumes random interaction between the oscillators and is easily seen where the oscillators are synchronous, or where there is some correlation between the oscillators and the system is of small dimension; different results can be produced as shown in Figure 11 in the left-hand side graph. In this example there are four oscillators with $\omega_1 = 1.012$, $\omega_2 = 0.992$, $\omega_3 = 1.021$, $\omega_4 = 1.000$, and Nosé mass 1.2, and we find that $\langle p_s^2/Q \rangle = 3.144$. Compare this result with the correct value $\langle p_s^2/Q \rangle = 1$ and the value predicted from (78) of $\langle p_s^2/Q \rangle = 4$. Clearly, in this case, thermostatting p_s should have a dramatic effect on the results, as seen in the right-hand side graph of Figure 11, where $\langle p_s^2/Q \rangle = 1.010$, leading to much faster convergence to the canonical ensemble.

4.3.2. Multiple oscillators in multiscale systems. In systems where there is no correlation between the oscillators, for example, in a multiscale system, we would expect the only interaction to be between the oscillators and the auxiliary variables. When sampling from the

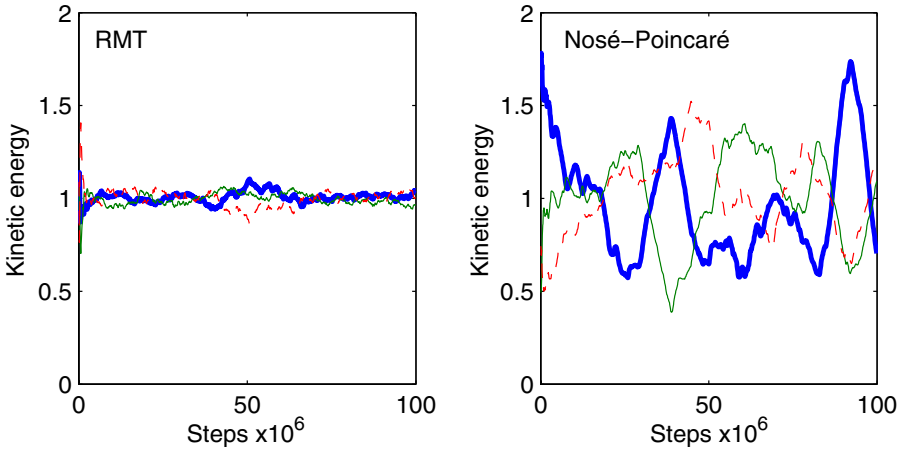

Figure 12. *Kinetic energy for three oscillators using RMT and Nosé–Poincaré methods for $kT = 1$.*

canonical ensemble, the lth oscillator would be expected to pass through the point $\tilde{p}_l = 0$, $q_l = 0$ at which point all of the energy for that oscillator must reside in the auxiliary variables, based on the assumption above. By separating s into dynamic and average values such that $s = \tilde{s}\langle s\rangle$, the auxiliary variable phase-space bound (62) can be rewritten, using (14), as

$$\frac{\tilde{p}_s^2}{2Q} + kT\ln\tilde{s} = \frac{\tilde{H}_0}{N_f} - kT\ln\langle s\rangle = kT. \tag{83}$$

From the above argument this is also an upper bound for the lth oscillator energy, and hence

$$\frac{\tilde{p}_l^2}{2m_l} + \frac{q_l^2}{2} \le kT. \tag{84}$$

Taking averages and noting that the sum of the energies of all oscillators is NkT yield

$$\left\langle \frac{\tilde{p}_l^2}{2m_l} + \frac{q_l^2}{2} \right\rangle = kT. \tag{85}$$

From this we anticipate that by thermostatting the thermostat, such that $\langle \tilde{p}_s^2/Q\rangle = kT$ and the auxiliary variable phase-space is bounded by (62), the equipartition of energy between the oscillators would be enforced. Using the RMT method in comparison to the standard Nosé–Poincaré method, we see that indeed this is the case as shown in Figure 12, where three oscillators with frequencies $\omega_1 = 1.000$, $\omega_2 = 0.308$, $\omega_3 = 0.095$, Nosé mass 8, and a step size 0.05 are simulated. The kinetic energies are calculated for each oscillator using running averages of 1,000,000 steps. Since the equipartition of energy can be shown for systems of harmonic oscillators which sample from the canonical ensemble, convergence to the canonical ensemble is considerably faster.

5. Conclusion. It is often assumed that Nosé's method works by using the Nosé mass to tune the self-oscillation frequency of the auxiliary variables to resonate with some natural

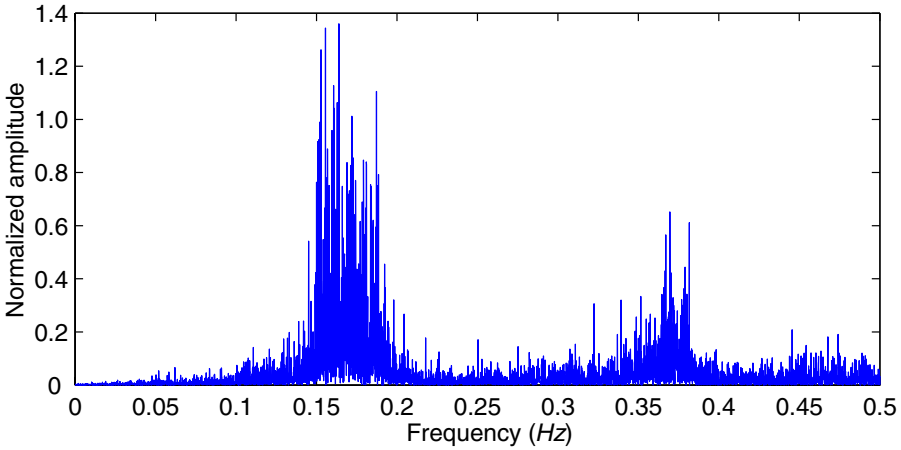

Figure 13. *Frequency domain plot of p_s for single harmonic oscillator, with frequency* $0.167Hz$*, sampling from the canonical ensemble.*

frequency within the system to be simulated. In fact, provided that the value of Q is large enough to prevent thermostat self-oscillation, the auxiliary variables will oscillate at the first harmonics of any frequencies within the system, introducing a potential 2:1 resonance, as shown on the model in section 2.3. These first harmonics persist as the system moves into the canonical ensemble (with additional oscillations at the fundamental frequencies, as seen in Figure 13, for an oscillator with frequency 0.167Hz showing the Fourier analysis of p_s) when interactions with the auxiliary variable phase-space boundary occur and coincide with more chaotic behavior of the system. It is clear that to sample from the canonical ensemble the phase-space variables must approach their boundary, and this can be induced by the correct choice of Q, or by controlling the thermostat so that its canonical ensemble average is achieved. In the latter case the recursive thermostatting technique has proven to overcome many of the difficulties of previous methods and generally requires fewer thermostats.

Recursive thermostatting has benefits in situations where the system consists of oscillators of similar frequencies, where Nosé dynamics leads to a large part of the auxiliary variable phase-space being sampled, and hence too great a value for $\langle p_s^2/Q \rangle$ giving incorrect sampling, and in multiscale systems, where the equipartition of energy, and hence isothermal behavior, is difficult to achieve. In addition, the large range of choice for the Nosé mass allows for the use of small masses, and hence fast thermostatting, which is useful for large systems where traditionally a large Nosé mass is required.

Appendix.

Hamiltonian splitting method for RMTs. The numerical methods used for the following experiments are based on the general Hamiltonian

$$H = \sum_{i=1}^{N} \frac{p_i^2}{2m_i} + V(q),$$

where $q = (q_1, \ldots, q_N)$. The RMT method derived from this, with M thermostats based on the auxiliary function in (73), is then

$$H_{NR} = \sum_{i=1}^{N} \frac{p_i^2}{2m_i s_1^2 \cdots s_M^2} + V(q) + \sum_{j=1}^{M-1} \frac{p_{s_j}^2}{2Q_j s_{j+1}^2 \cdots s_M^2} + \frac{p_{s_M}^2}{2Q_M} + gkT \ln s_1 + \sum_{j=2}^{M} \left((N_f + j - 1)kT \ln s_j + \frac{(a_j - s_j)^2}{2C_j} \right),$$

where $g = N_f + 1$, giving a Nosé–Poincaré multiple thermostat method, with $g = N_f$,

$$H_{NPR} = s_1 s_2 \cdots s_M \left[H_{NR} - H_0 \right],$$

where H_0 is chosen as the initial value of H_{NR}. The equations of motion are

$$\begin{aligned}
\dot{q}_i &= \frac{p_i}{m_i s_1 \cdots s_M}, \\
\dot{p}_i &= -s_1 \cdots s_M \frac{\partial V(q)}{\partial q_i}, \\
\dot{s}_1 &= \frac{s_1 \cdots s_M p_{s_1}}{Q_1 s_2^2 \cdots s_M^2}, \\
\dot{p}_{s_1} &= s_2 \cdots s_M \left(\sum_{i=1}^{N} \frac{p_i^2}{m_i s_1^2 \cdots s_M^2} - N_f kT - H_{NR}(q, p, s, \hat{p}_s) + H_0 \right), \\
\dot{s}_j &= \frac{s_1 \cdots s_M p_{s_j}}{Q_j s_{j+1}^2 \cdots s_M^2}, \\
\dot{p}_{s_j} &= s_1 \cdots s_M \left(\sum_{i=1}^{N} \frac{p_i^2}{m_i s_1^2 \cdots s_j^3 \cdots s_M^2} + \sum_{l=1}^{j-1} \frac{p_{s_l}^2}{Q_l s_{l+1}^2 \cdots s_j^3 \cdots s_M^2} \right. \\
&\qquad \left. - \frac{(N_f + j - 1)kT}{s_j} + \frac{a_j - s_j}{C_j} - \frac{H_{NR}(q, p, s, \hat{p}_s) - H_0}{s_j} \right), \quad 1 < j < M, \\
\dot{s}_M &= \frac{s_1 \cdots s_M p_{s_M}}{Q_M}, \\
\dot{p}_{s_M} &= s_1 \cdots s_M \left(\sum_{i=1}^{N} \frac{p_i^2}{m_i s_1^2 \cdots s_{M-1}^2 s_M^3} + \sum_{l=1}^{M-1} \frac{p_{s_l}^2}{Q_l s_{l+1}^2 \cdots s_{M-1}^2 s_M^3} \right. \\
&\qquad \left. - \frac{(N_f + M - 1)kT}{s_M} + \frac{a_M - s_M}{C_M} - \frac{H_{NR}(q, p, s, \hat{p}_s) - H_0}{s_M} \right),
\end{aligned}$$

where $s = (s_1, \ldots, s_M)$, $\hat{p}_s = (p_{s_1}, \ldots, p_{s_M})$, and $p = (p_1, \ldots, p_N)$. The thermostats have introduced an implicit coupling into the equations of motion, but an explicit method can be formulated by splitting the Hamiltonian and corresponding Liouville operator. For M thermostats this can be done using $2 + M$ Hamiltonians by employing a separate Hamiltonian for each extended variable "kinetic" term. Then if

$$H = H_1 + H_2 + H_{3_1} + \cdots + H_{3_M},$$

then we have

$$
\begin{aligned}
H_1 &= s_1 \cdots s_M \left[\sum_{i=1}^{N} \frac{p_i^2}{2m_i s_1^2 \cdots s_M^2} + N_f kT \ln s_1 \right], \\
H_2 &= s_1 \cdots s_M \left[V(q) + \sum_{j=2}^{M} \left((N_f + j - 1) kT \ln s_j + \frac{(a_j - s_j)^2}{2C_j} \right) \right], \\
H_{3_1} &= s_1 \cdots s_M \left[\frac{p_{s_1}^2}{2Q_1 s_2^2 \cdots s_M^2} - H_0 \right], \\
H_{3_j} &= s_1 \cdots s_M \left[\frac{p_{s_j}^2}{2Q_j s_{j+1}^2 \cdots s_M^2} \right], \quad 1 < j < M, \\
H_{3_M} &= s_1 \cdots s_M \left[\frac{p_{s_M}^2}{2Q_M} \right].
\end{aligned}
$$

Using a symmetric splitting of the Liouville operator to get a symplectic and time reversible method,

$$
\begin{aligned}
iL_H &= \{., H\} \\
&= \{., H_1\} + \{., H_2\} + \{., H_{3_1}\} + \cdots + \{., H_{3_M}\} \\
&= iL_{H_1} + iL_{H_2} + iL_{H_{3_1}} + \cdots + iL_{H_{3_M}}.
\end{aligned} \tag{86}
$$

This splitting introduces an error of order $\triangle t^3$ at each step in terms of the solution operator, giving a second order method,

$$
\begin{aligned}
\Psi_H(\triangle t) &= e^{iL_H \triangle t} \\
&= e^{iL_{H_2} \triangle t/2} e^{iL_{H_{3_1}} \triangle t/2} \cdots e^{iL_{H_{3_M}} \triangle t/2} e^{iL_{H_1} \triangle t} e^{iL_{H_{3_M}} \triangle t/2} \\
&\quad \cdots e^{iL_{H_{3_1}} \triangle t/2} e^{iL_{H_2} \triangle t/3} + O(\triangle t^3).
\end{aligned}
$$

The dynamics for H_1 and H_2 can be solved in a straightforward manner, leaving $H_{3_1} \cdots H_{3_M}$ to be solved either analytically or by using the generalized leapfrog algorithm as described in [2].

Acknowledgments. The authors wish to thank Zhidong Jia, Brian Laird, and Frederic Legoll for their valuable comments and suggestions during the preparation of this paper.

REFERENCES

[1] H. Andersen, *Molecular dynamics simulations at constant pressure and/or temperature*, J. Chem. Phys., 72 (1980), pp. 2384–2393.

[2] S. Bond, B. Leimkuhler, and B. Laird, *The Nosé-Poincaré method for constant temperature molecular dynamics*, J. Comput. Phys., 151 (1999), pp. 114–134.

[3] C. Dettmann, *Hamiltonian for a restricted isoenergetic thermostat*, Phys. Rev. E (3), 60 (1999), pp. 7576–7577.

[4] F. DiTolla and M. Ronchetti, *Applicability of nos isothermal reversible dynamics*, Phys. Rev. E (3), 48 (1993), pp. 1726–1737.
[5] E. Hernández, *Metric-tensor flexible-cell algorithm for isothermal isobaric molecular dynamics simulations*, J. Chem. Phys., 115 (2001), pp. 10282–10290.
[6] W. Hoover, *Canonical dynamics: Equilibrium phase-space distributions*, Phys. Rev. A, 31 (1985), pp. 1695–1697.
[7] W. Hoover, K. Aoki, C. Hoover, and S. DeGroot, *Time-reversible deterministic thermostats*, Phys. D, 187 (2004), pp. 253–267.
[8] Z. Jia and B. Leimkuhler, *Partial thermostatting molecular dynamics for slow-fast mixture problems*, J. Multiscale Modeling and Simulation, submitted.
[9] D. Kusnezov, A. Bulgac, and W. Bauer, *Canonical ensembles from chaos i: Classical systems*, Ann. Physics, 204 (1990), pp. 155–185.
[10] B. Laird and B. Leimkuhler, *A generalized dynamical thermostatting technique*, Phys. Rev. E (3), 68 (2003), p. 16704.
[11] B. Laird and J. Sturgeon, *Symplectic algorithm for constant-pressure molecular dynamics using a Nosé-Poincaré thermostat*, J. Chem. Phys., 112 (2000), pp. 3474–3482.
[12] B. Leimkuhler and C. Sweet, *The canonical ensemble via symplectic integrators using Nosé and Nosé-Poincaré chains*, J. Chem. Phys., 12 (2004), pp. 108–116.
[13] G. Martyna, M. Klein, and M. Tuckerman, *Nosé-Hoover chains: The canonical ensemble via continuous dynamics*, J. Chem. Phys., 97 (1992), pp. 2635–2643.
[14] S. Nosé, *A molecular dynamics method for simulation in the canonical ensemble*, Mol. Phys., 52 (1984), pp. 255–268.
[15] S. Nosé, *An improved symplectic integrator for Nosé-Poincaré thermostat*, J. Phys. Soc. Japan, 70 (2001), pp. 75–77.